DFT Study of the Ethylene Hydroformylation Catalytic Cycle Employing a HRh(PH₃)₂(CO) Model Catalyst

Stephen A. Decker and Thomas R. Cundari*

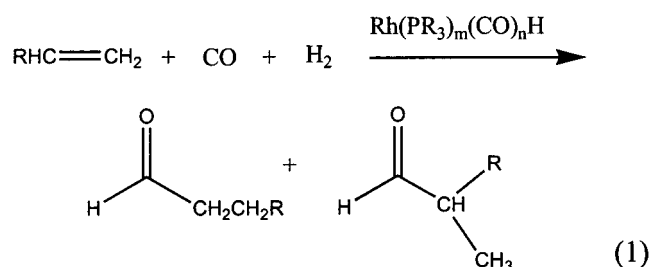*Computational Research on Materials Institute (CROMIUM), Department of Chemistry, The University of Memphis, Memphis, Tennessee 38152-3550*

The potential energy hypersurface for ethylene hydroformylation catalyzed by HRh(PH₃)₂-(CO) was mapped out at the CCSD(T)//B3LYP and B3LYP//B3LYP levels of theory using effective core potentials. Combining the results obtained for each elementary step there are a number of possible pathways for the hydroformylation catalytic cycle, originating from the trans (**2a**) and cis (**2b**) isomers of the active catalyst. At both levels of theory employed, a preference was predicted for the pathways originating from the trans isomer of the active catalyst, **2a**. The alternative pathways originating from the cis isomer, **2b**, were discounted because of the large activation barriers predicted for the two migratory insertion reactions, arising from unfavorable interactions between the equatorial phosphine ligands and the migrating axial ligand. Considering only those reaction paths originating from the trans isomer of the active catalyst, **2a**, a strong preference was identified for the oxidative addition of H₂ to the unsaturated Rh-acyl complex (**6a**) on the same side as the ethyl moiety of the acyl ligand, as opposed to the addition on the opposite face (i.e., on the same side as the acyl oxygen). In the final aldehyde reductive elimination step an energetic preference was predicted for the migration of the hydride ligand trans to the CO ligand in the most stable H₂ oxidative addition products; however, this migration would lead to the generation of the cis catalyst instead of the trans catalyst. Therefore, either the less electronically favored hydride ligand trans to the PH₃ ligand migrates to the acyl carbon, thereby regenerating **2a**, or there must be some interconversion between the pathways originating from **2a** and **2b**. This interconversion would most likely occur at either the η²-olefin adduct (**3b**) or the CO addition intermediate (**5b**), since previous research indicates that complexes of this type can undergo facile pseudorotation. For the energetically feasible catalytic cycle, the CO insertion step is predicted to be the rate-determining step with predicted activation barriers of 20.4 and 14.9 kcal/mol, at the CCSD(T)//B3LYP and B3LYP//B3LYP levels of theory, respectively. The experimental enthalpy of hydroformylation (−28 kcal/mol), corresponding to the energy difference between the end aldehyde product and the constituent reactant species, C₂H₄, CO, and H₂, is overestimated by about 7 kcal/mol (−34.7 kcal/mol) at the B3LYP//B3LYP level. However, recomputing the energies of the species with the CCSD(T) methodology yields a value of −24.4 kcal/mol, which is more in accord with experiment.

Introduction

Hydroformylation involves the conversion of an olefin, CO, and H₂ into the corresponding aldehyde (eq 1), and it is one of the largest industrial processes (millions of tons annually) catalyzed by a homogeneous transition metal complex.[1] If terminal olefins other than ethylene

$$(1)$$

are used, then both the linear and branched aldehyde are produced, although the linear aldehydes are more

desirable industrially, since they are typically converted into detergent alcohols.[2,3]

The most popular hydroformylation catalysts employed in industry are the low-valent Co and Rh catalysts,[2,3] although a number of other catalysts based on Pt, Ru, Ir, and Pd are utilized in asymmetric hydroformylation.[4] The original homogeneous hydroformylation catalyst employed by Roelen[5] was Co₂(CO)₈, which generates the HCo(CO)₄ catalyst precursor in situ. The dissociation of one of the CO ligands yields the HCo(CO)₃ active catalyst and initiates hydroformylation. The rhodium analogues of the simple cobalt

---

(1) Parshall, G. W.; Ittel, S. D. *Homogeneous Catalysis*, 2nd ed.; Wiley: New York, 1992.
(2) Collman, J. P.; Hegedus, L. S.; Norton, J. R.; Finke, R. G. *Principles and Applications of Organotransition Metal Chemistry*; University Science Books: Mill Valley, CA, 1987.
(3) Crabtree, R. H. *The Organometallic Chemistry of the Transition Metals*; Wiley: New York, 1988.
(4) Agbossou, F.; Carpentier, J.-F.; Mortreux, A. *Chem. Rev.* **1995**, *95*, 2485.
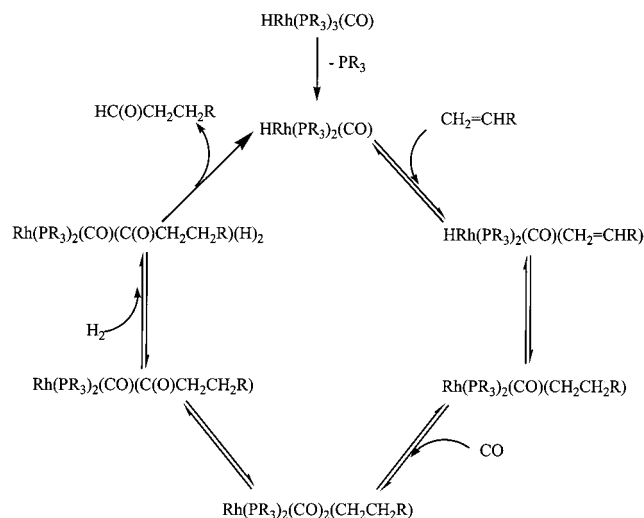(5) Roelen, O. *Chem. Zentr.* **1953**, 927.

* Address correspondence to this author.

carbonyls, $Rh_4(CO)_{12}$ and $Rh_6(CO)_{16}$, which generate $HRh(CO)_4$ under high CO/H_2 pressure, are also very active hydroformylation catalysts. Unfortunately, these rhodium carbonyl catalysts tend to actively catalyze the competing olefin hydrogenation and isomerization reactions and produce lower yields of the desired linear aldehydes than their cobalt counterparts.[2] It was later observed that the replacement of one or more of the CO ligands with a phosphine, such as $P(^nBu)_3$, results in higher linear:branched aldehyde product ratios.[6] The increased steric bulk of the phosphines is believed to favor the formation of the less hindered linear alkyl complexes during the olefin insertion step, the key step in determining the regiochemistry of the final aldehyde product. The phosphine-modified rhodium carbonyl systems, $HRh(PR_3)_m(CO)_n$; $m = 1$, $n = 2$ or $m = 2$, $n = 1$, are very active hydroformylation catalysts that exhibit a high degree of selectivity for the desired linear aldehyde product.[7-11] This regioselectivity, however, does show a strong dependence on the CO pressure and phosphine concentration.[9] Generally, the bisphosphine monocarbonyl catalyst, $HRh(PR_3)_2(CO)$, displays a higher regioselectivity than the corresponding monophosphine biscarbonyl catalyst, $HRh(PR_3)(CO)_2$. However, the larger steric demand of $HRh(PR_3)_2(CO)$ is believed to make the olefin addition step slower than that for $HRh(PR_3)(CO)_2$. Typically, these two active catalyst systems exist in equilibrium. The position of this equilibrium is influenced by the phosphine concentration and CO pressure. Under the usual industrial conditions of high phosphine concentration and low CO pressure, the equilibrium shifts toward the $HRh(PR_3)_2(CO)$ catalyst.[8]

The widely accepted mechanism for olefin hydroformylation employing the $HRh(PR_3)_2(CO)$ catalysts was originally proposed in 1970 by Wilkinson et al.,[7-11] and it is displayed in Scheme 1. Wilkinson's hydroformylation catalytic cycle is comprised of seven elementary reactions: catalyst generation, olefin addition, olefin insertion, CO addition, CO insertion, H_2 oxidative addition, and aldehyde reductive elimination. The regioselectivity of the aldehyde is determined in the olefin insertion step, and experimental evidence suggests that the H_2 oxidative addition step is rate-limiting.

Hydroformylation has received a lot of attention from the computational chemistry community, due to its industrial importance. As detailed in the recent reviews by Torrent et al.,[12] numerous researchers have investigated some or all of the elementary reactions of the catalytic cycle. The mechanistic details of the $HCo(CO)_4$-catalyzed hydroformylation process have been examined by a number of researchers including Grima et al.,[13] Antolovic and Davidson,[14-16] Veillard et al.,[17,18] and

Scheme 1.   Wilkinson's Hydroformylation Catalytic Cycle

Ziegler and co-workers.[19-24] These modeling studies were carried out at a variety of different levels of theory ranging from the CNDO/2 semiempirical approach employed by Grima and co-workers, to the correlated wave function-based methods employed by the Davidson and Veillard groups, to the density functional theory (DFT) method employed by Ziegler's group. Frenking and co-workers explored a number of the elementary steps of hydroformylation catalyzed by $HRh(CO)_4$ at the MP2 level of theory.[25] Frenking et al. have also examined the catalyst generation step in the olefin hydroformylation catalyzed by the phosphine-substituted rhodium carbonyl catalyst system. In this study they focused on the catalyst initiation reaction leading to the two active catalyst systems, $HRh(PR_3)_2(CO)$ and $HRh(PR_3)(CO)_2$, at a variety of different levels of theory.[26] Finally, in a collection of impressive papers, Morokuma and co-workers have examined the hydroformylation of ethylene by a $HRh(PH_3)(CO)_2$ active catalyst.[27-31] In their MP2//RHF study, they were able to construct the entire potential energy hypersurface for the ethylene hydroformylation catalytic cycle. In addition, they found that solvation of the unsaturated intermediates had

(6) Slaugh, L. H.; Mullineaux, R. D. *J. Organomet. Chem.* **1968**, *13*, 469.
(7) Osborn, J. A.; Wilkinson, G.; Young, J. F. *Chem. Commun.* **1965**, 17.
(8) Evans, D.; Yagupsky, G.; Wilkinson, G. *J. Chem. Soc. A* **1968**, 2660.
(9) Evans, D.; Osborn, J. A.; Wilkinson, G. *J. Chem. Soc. A* **1968**, 3133.
(10) Yagupsky, G.; Brown, C. K.; Wilkinson, G. *J. Chem. Soc. A* **1970**, 1392.
(11) Brown, C. K.; Wilkinson, G. *J. Chem. Soc. A* **1970**, 2753.
(12) Torrent, M.; Sola, M.; Frenking, G. *Chem. Rev.* **2000**, *100*, 439.
(13) Grima, J. P.; Choplin, F.; Kaufman, G. *J. Organomet. Chem.* **1977**, *129*, 221.
(14) Antolovic, D.; Davidson, E. R. *J. Am. Chem. Soc.* **1987**, *109*, 977.
(15) Antolovic, D.; Davidson, E. R. *J. Am. Chem. Soc.* **1987**, *109*, 5828.
(16) Antolovic, D.; Davidson, E. R. *J. Chem. Phys.* **1988**, *88*, 4967.
(17) Veillard, A.; Strich, A. *J. Am. Chem. Soc.* **1988**, *110*, 3793.
(18) Veillard, A.; Daniel, C.; Rohmer, M.-M. *J. Phys. Chem.* **1990**, *94*, 5556.
(19) Versluis, L.; Ziegler, T.; Baerends, E. J.; Ravenek, W. *J. Am. Chem. Soc.* **1989**, *111*, 2018.
(20) Versluis, L.; Ziegler, T. *Organometallics* **1990**, *9*, 2985.
(21) Versluis, L.; Ziegler, T.; Fan, L. *Inorg. Chem.* **1990**, *29*, 4530.
(22) Ziegler, T. *Pure Appl. Chem.* **1991**, *63*, 873.
(23) Ziegler, T.; Cavallo, L.; Berces, A. *Organometallics* **1993**, *12*, 3586.
(24) Sola, M.; Ziegler, T. *Organometallics* **1996**, *15*, 2611.
(25) Pidun, U.; Frenking, G. *Chem. Eur. J.* **1998**, *4*, 522.
(26) Schmid, R.; Herrmann, W. A.; Frenking, G. *Organometallics* **1997**, *16*, 701.
(27) Koga, N.; Jin, S. Q.; Morokuma, K. *J. Am. Chem. Soc.* **1988**, *110*, 3417.
(28) Koga, N.; Morokuma, K. *Top. Phys. Organomet. Chem.* **1989**, *3*, 1.
(29) Musaev, D. G.; Matsubara, T.; Mebel, A. M.; Koga, N.; Morokuma, K. *Pure Appl. Chem.* **1995**, *67*, 257.
(30) Musaev, D. G.; Morokuma, K. In *Advances in Chemical Physics*; Prigogine, I., Rice, S. A., Eds.; Wiley: New York, 1996; Vol. 95, p 61.
(31) Matsubara, T.; Koga, N.; Ding, Y.; Musaev, D. G.; Morokuma, K. *Organometallics* **1997**, *16*, 1065.

a profound effect on the energetics of the catalytic cycle, although only a single ethylene molecule was used to simulate the microsolvation effects of the ethylene solvent. In addition to these ab initio and DFT modeling studies, a number of researchers have employed lower level computational methods, like molecular mechanics[32-35] and the Fenske–Hall method,[36] to study various aspects of hydroformylation, particularly the regioselectivity.

The current paper focuses on ethylene hydroformylation catalyzed by a bisphosphine monocarbonyl rhodium catalyst system, in this case a HRh(PH₃)₂(CO) model catalyst. Nonlocal, gradient-corrected DFT, in conjunction with effective core potentials and valence basis sets, was utilized to locate all of the stationary points in the catalytic cycle. DFT incorporates electron correlation effects in a straightforward manner and is known to predict accurate molecular structures and energetics for organometallics, at a fraction of the computational expenditure of the correlated ab initio wave function-based methods.[37,38] The high level, ab initio CCSD(T) method[39-44] was employed to compute the energies of all of the stationary points, to refine the energetics of the potential energy hypersurface. Frenking et al.[45] have shown that this CCSD(T)//DFT approach yields accurate reaction energetics for organometallic systems. The present study seeks to extend the understanding of the intricate structural and energetic details of the olefin hydroformylation process and will enable a direct comparison to the previous results obtained for the HRh(PR₃)(CO)₂ catalyst system.

Computational Methods

The entire gas-phase potential energy hypersurface for the ethylene hydroformylation catalytic cycle initiated from a HRh(PR₃)₂(CO) active catalyst was determined at the CCSD(T)//B3LYP and B3LYP//B3LYP levels of theory. To reduce the computational complexity of the calculations, a PH₃ model phosphine ligand was used in lieu of PPh₃ and related phosphine ligands typically found in experimental systems. Although PMe₃ has been shown to be a better model of PPh₃ than PH₃,[26] it was felt that the additional degrees of freedom arising from the methyl groups would inhibit a thorough investigation of the different isomers and conformers of each species participating in the catalytic cycle.

The B3LYP hybrid density functional was employed for all of the DFT calculations. This functional is comprised of Becke's hybrid gradient-corrected exchange functional[46] and the gradient-corrected correlation functional of Lee, Yang, and Parr.[47] The effective core potential (ECP) valence basis set of Stevens et al.[48-50] was employed for Rh and the main group atoms. For Rh, the small core ECPs were employed, and thus a total of 17 electrons were included in the valence space and treated explicitly in the calculation. The associated Rh valence basis set employed in the calculations was of triple-ζ valence quality and had the following contraction scheme: (4211/4211/311). Only the outermost valence electrons (i.e., the ns and np electrons) of the main group atoms were treated explicitly in the calculations, and the valence basis set employed was of double-ζ plus polarization quality, having a (31/31/1*) contraction pattern. The single d-polarization function was taken from the collection of Huzinaga and co-workers.[51] The standard -31G contracted basis set was employed for all of the hydrogen atoms in the calculations.[52] This basis set will hereafter be denoted as SBK(d).

The geometries of all of the species participating in the ethylene hydroformylation catalytic cycle were fully optimized using analytical gradient techniques at the B3LYP level of theory. Whenever possible, symmetry constraints were imposed during the optimizations in an effort to reduce the computational expense. All of the resultant optimized stationary points were characterized via harmonic vibrational analysis, at the B3LYP level, using either analytical energy second derivatives or numerical differentiation of the analytical energy first derivatives. Zero-point energy corrections, derived from the B3LYP harmonic vibrational frequencies, were added to the total energies of each species in the catalytic cycle. The Gaussian98[53] and NWChem[54] program suites were employed for all of the DFT calculations in this study.

To refine the energetics of the catalytic cycle, CCSD(T) single point energy calculations, utilizing the same SBK(d) basis set, were performed for each species participating in the catalytic cycle, at their respective B3LYP optimized geometries (i.e., CCSD(T)/SBK(d)//B3LYP/SBK(d)). The Gaussian98 program package was employed for all of these CCSD(T) single point energy calculations.

Results and Discussion

The hydroformylation of ethylene following Wilkinson's mechanistic scheme involves alternating trigonal bipyramidal and square-planar complexes. The H₂

(32) Castonguay, L. A.; Rappe, A. K.; Casewit, C. J. *J. Am. Chem. Soc.* **1991**, *113*, 7177.

(33) Kronenberg, M.; van der Burgt, Y. E. M.; Kamer, P. C. J.; van Leeuwen, P. W. N. M. *Organometallics* **1995**, *14*, 3081.

(34) Casey, C. P.; Petrovich, L. M. *J. Am. Chem. Soc.* **1995**, *117*, 6007.

(35) Gleich, D.; Schmid, R.; Herrmann, W. A. *Organometallics* **1998**, *17*, 2141.

(36) Trzeciak, A. M.; Szterenberg, L.; Wolszczak, E.; Ziolkowski, J. J. *J. Mol. Catal. A* **1995**, *99*, 23.

(37) Ziegler, T. *Chem. Rev.* **1991**, *91*, 651.

(38) Ziegler, T. *Can. J. Chem.* **1995**, *73*, 743.

(39) Cizek, J. *J. Chem. Phys.* **1966**, *45*, 4256.

(40) Pople, J. A.; Krishnan, R.; Schlegel, H. B.; Binkley, J. S. *Int. J. Quantum Chem.* **1978**, *14*, 545.

(41) Bartlett, R. J.; Purvis, G. D. *Int. J. Quantum Chem.* **1978**, *14*, 561.

(42) Purvis, G. D.; Bartlett, R. J. *J. Chem. Phys.* **1982**, *76*, 1910.

(43) Raghavachari, K.; Trucks, G. W.; Pople, J. A.; Head-Gordon, M. *Chem. Phys. Lett.* **1989**, *157*, 479.

(44) Bartlett, R. J.; Watts, J. D.; Kucharski, S. A.; Noga, J. *Chem. Phys. Lett.* **1990**, *165*, 513.

(45) Frenking, G.; Antes, I.; Bohme, M.; Dapprich, S.; Ehlers, A. W.; Jonas, V.; Neuhaus, A.; Otto, M.; Stegmann, R.; Veldkamp, A.; Vyboishchikov, S. F. In *Reviews in Computational Chemistry*; Lipkowitz, K. B., Boyd, D. B., Eds.; VCH: New York, 1996; Vol. 8, p 63.

(46) Becke, A. D. *J. Chem. Phys.* **1993**, *98*, 5648.

(47) Lee, C.; Yang, W.; Parr, R. G. *Phys. Rev. B* **1988**, *37*, 785.

(48) Stevens, W. J.; Basch, H.; Krauss, M. *J. Chem. Phys.* **1984**, *81*, 6026.

(49) Stevens, W. J.; Basch, H.; Krauss, M.; Jasien, P. *Can. J. Chem.* **1992**, *70*, 612.

(50) Cundari, T. R.; Stevens, W. J. *J. Chem. Phys.* **1993**, *98*, 5555.

(51) Huzinaga, S.; Andzelm, J.; Klobukowski, M.; Radzio-Andzelm, E.; Sakai, Y.; Tatewaki, H. *Gaussian Basis Sets for Molecular Calculations*; Elsevier: Amsterdam, 1984.

(52) Ditchfield, R.; Hehre, W. J.; Pople, J. A. *J. Chem. Phys.* **1971**, *54*, 724.

(53) Frisch, M. J.; Trucks, G. W.; Schlegel, H. B.; Scuseria, G. E.; Robb, M. A.; Cheeseman, J. R.; Zakrzewski, V. G.; Montgomery, J., J. A.; Stratmann, R. E.; Burant, J. C.; Dapprich, S.; Millam, J. M.; Daniels, A. D.; Kudin, K. N.; Strain, M. C.; Farkas, O.; Tomasi, J.; Barone, V.; Cossi, M.; Cammi, R.; Mennucci, B.; Pomelli, C.; Adamo, C.; Clifford, S.; Ochterski, J.; Petersson, G. A.; Ayala, P. Y.; Cui, Q.; Morokuma, K.; Malick, D. K.; Rabuck, A. D.; Raghavachari, K.; Foresman, J. B.; Cioslowski, J.; Ortiz, J. V.; Stefanov, B. B.; Liu, G.; Liashenko, A.; Piskorz, P.; Komaromi, I.; Gomperts, R.; Martin, R. L.; Fox, D. J.; Keith, T.; Al-Laham, M. A.; Peng, C. Y.; Nanayakkara, A.; Gonzalez, C.; Challacombe, M.; Gill, P. M. W.; Johnson, B.; Chen, W.; Wong, M. W.; Andres, J. L.; Gonzalez, C.; Head-Gordon, M.; Replogle, E. S.; Pople, J. A. *Gaussian 98*, Revision A.6; Gaussian, Inc.: Pittsburgh, PA, 1998.

(54) Bernholdt, D. E.; Apra, E.; Fruchtl, H. A.; Guest, M. F.; Harrison, R. J.; Kendall, R. A.; Kutteh, R. A.; Long, X.; Nicholas, J. B.; Nichols, J. A.; Taylor, H. L.; Wong, A. T.; Fann, G. I.; Littlefield, R. J.; Nieplocha, J. *Int. J. Quantum Chem. Symp.* **1995**, *29*, 475.
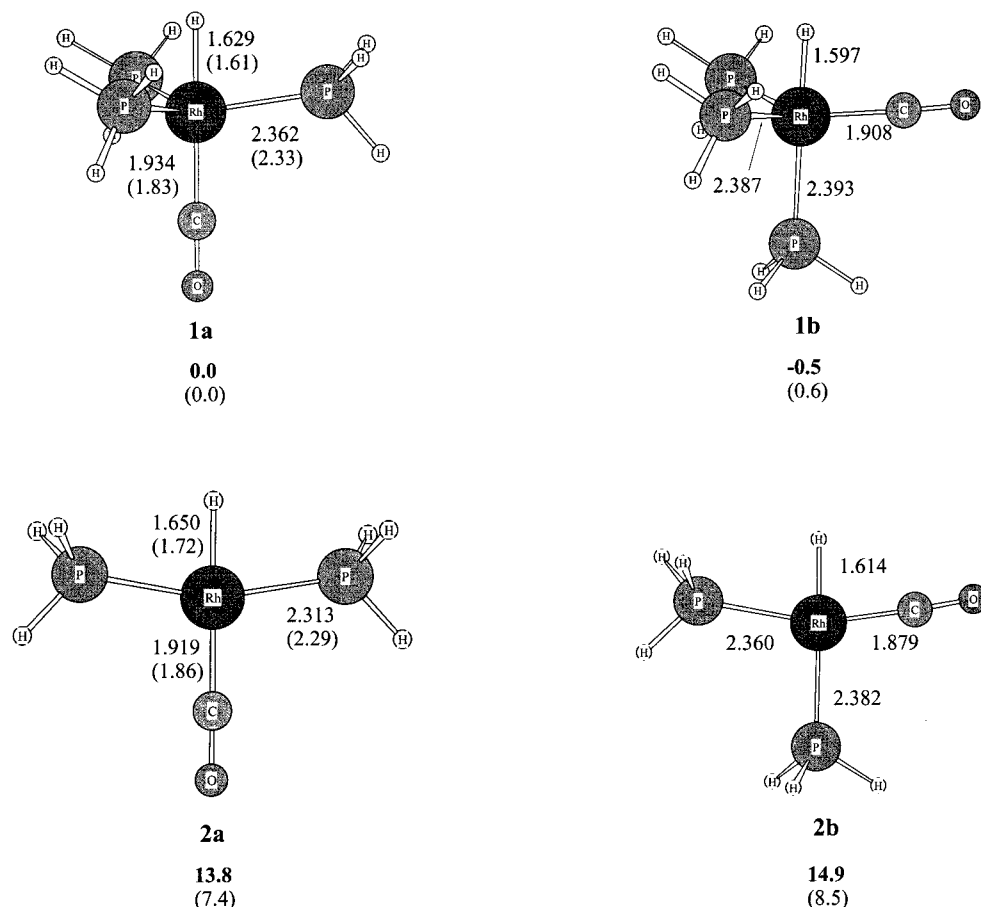
Figure 1. Structural and energetic data for the species involved in the catalyst generation step (catalyst precursors, **1a** and **1b**; the active catalysts, **2a** and **2b**). Energy values given in bold correspond to the CCSD(T)//B3LYP relative energies (in kcal/mol), while those in parentheses correspond to the B3LYP//B3LYP relative energies. All geometric parameters were optimized at the B3LYP/SBK(d) level of theory, and where available the corresponding experimental values are given in parentheses. All distances are in angstroms, and angles in degrees.

oxidative addition step is an exception, since the Rh-acyl dihydride products are saturated octahedral complexes. Although there are a total of seven elementary reactions in the catalytic cycle, three of them involve the dissociation or association of a ligand for which we did not attempt to locate transition states (TSs). Transition states were obtained for the remaining four reactions: olefin insertion, CO insertion, H_2 oxidative addition, and aldehyde reductive elimination. Each step of the catalytic cycle was thoroughly investigated by examining all of the reasonable isomers and conformers of the various intermediates and TSs.

In the following sections the results for each elementary step of the catalytic cycle are presented first. Subsequently, the results are combined in order to construct the potential energy hypersurface for the entire catalytic cycle, which is discussed in the final section.

In the following discussion all of the intermediate species were characterized as local minima on their respective potential energy hypersurfaces based on their respective B3LYP/SBK(d) harmonic vibrational frequencies, unless otherwise noted. In addition, each optimized TS contained a single imaginary harmonic vibrational frequency, as required to characterize it as a true TS. When necessary, the details of the harmonic vibrational frequency calculations are discussed in more detail.

In the following sections all of the energetic values,

both relative energies and activation barriers, correspond to the CCSD(T)//B3LYP computed values, with the corresponding B3LYP//B3LYP values given in parentheses (i.e., the CCSD(T) (B3LYP) notation). Furthermore, all of the CCSD(T) and B3LYP energies include the zero-point energy correction, derived from the B3LYP/SBK(d) harmonic vibrational frequencies.

1. Catalyst Generation Step. The first step in the hydroformylation of ethylene is the generation of the 16-electron, unsaturated active catalyst species via ligand dissociation from a precursor. As discussed earlier, the precursor is either $HRh(PR_3)_3(CO)$ or $HRh(PR_3)_2(CO)_2$ and the active catalyst, in this case $HRh(PR_3)_2(CO)$, can be generated via PR_3 dissociation from the former or CO dissociation from the latter. In the present study the PR_3 dissociation process was investigated.

The calculated structural and energetic data for the precursor and active catalyst species are given in Figure 1. Experimental metric parameters for the related $HRh(PPh_3)_3(CO)$ and $HRh(PCy_3)_2(CO)$ complexes[55-57] are given in parentheses in Figure 1. Our investigations were restricted to the trigonal bipyramidal precursor structures, as these have been shown in previous studies

(55) LaPlaca, S. J.; Ibers, J. A. *Acta Crystallogr.* **1965**, *18*, 511.
(56) Babra, I. S.; Morley, L. S.; Nyburg, S. C.; Parkins, A. W. *J. Cryst. Spectrosc.* **1993**, *23*, 997.
(57) Freeman, M. A.; Young, D. A. *Inorg. Chem.* **1986**, *25*, 1556.

to be the most stable coordination geometry. Furthermore, only structures with an axial hydride ligand were examined, since this is known, by both experiment and theory, to be the preferred coordination site.[58,59]

As seen in Figure 1 there are two possible precursor isomers: with the hydride ligand trans to the CO ligand (labeled **1a**) or with the hydride ligand cis to the CO ligand (labeled **1b**). The CCSD(T)//B3LYP and B3LYP//B3LYP calculations predict the two isomers to be roughly isoenergetic, with less than 1 kcal/mol separating them. A comparison of the predicted molecular geometries of the two isomers reveals that the Rh–H bond is longer by 0.03 Å in **1a** than in **1b**, as may be expected due to the stronger trans influence of the CO ligand compared to that of the PH₃ ligand.

The dissociation of one of the equatorial PH₃ ligands from the two precursors leads to the 16-electron catalysts, denoted as **2a** and **2b** (see Figure 1). At both the CCSD(T)//B3LYP and B3LYP//B3LYP levels there is a slight energetic preference, by 1.1 kcal/mol, for the isomer in which the hydride ligand is trans to the CO ligand, **2a**. Phosphine dissociation from **1a** and **1b** is predicted to be endothermic by 13.8 (7.4) and 15.4 (7.9) kcal/mol, respectively. This value for **1a** → **2a** + PH₃ agrees nicely with Frenking's previous CCSD(T)//MP2 value of 11.9 kcal/mol;[26] however, it underestimates the experimental ΔH value of 20 ± 1 kcal/mol found for the dissociation of PPh₃ from HRh(PPh₃)₃(CO).[60] This difference may be attributed to the electronic and steric differences between the model PH₃ ligand employed in the calculations and the experimental PPh₃ ligand. Interestingly, Morokuma et al.[31] computed much larger dissociation energies, of 20–25 kcal/mol at the MP2//RHF level of theory, for the dissociation of PH₃ from HRh(PH₃)₂(CO)₂ leading to the HRh(PH₃)(CO)₂ active catalyst.

As seen in Figure 1, phosphine dissociation induces a slight lengthening of the Rh–H bond distance, by about 0.01–0.02 Å, and a reduction of the Rh–P and Rh–CO bonds, by 0.01–0.05 and 0.02–0.03 Å, respectively. The shortening of the Rh–P bond length is consistent with the available experimental crystal structure data for HRh(PPh₃)₃(CO) and HRh(PCy₃)₂(CO); however, based on this crystal structure data the Rh–CO distance is slightly longer in the unsaturated complex.

The B3LYP geometric parameters for **1a** and **2a** agree quite well with the corresponding experimental values for HRh(PPh₃)₃(CO) and HRh(PCy₃)₂(CO). For the precursor species, **1a**, the B3LYP-predicted Rh–H and Rh–P bond lengths overestimate the corresponding experimental values by 0.01–0.03 Å, while the Rh–C bond length is overestimated by 0.10 Å. Comparison of the experimental and B3LYP optimized geometric parameters for the unsaturated square-planar complexes reveals that the Rh–P and Rh–C bond distances are predicted to be too long by 0.02 and 0.06 Å while the Rh–H distance is predicted to be too short, by 0.07 Å, at the B3LYP level. In both **1a** and **2a** the B3LYP optimized structures correctly reproduce the bending of

the cis ligands toward the hydride ligand, by 8–9°. Since this phenomenon is found with the bulkier experimental PR₃ ligands and the relatively small PH₃ model ligands, this tendency can most likely be attributed to electronics instead of sterics.[26]

2. Olefin Addition. Once generated, the active catalyst coordinates the olefin, in this case ethylene, to form an η^2-olefin adduct. B3LYP optimizations were carried out for the two possible coordination isomers of the η^2-ethylene adducts, with the ethylene coordinated in either the equatorial or axial position. A strong energetic preference (of 7.7 kcal/mol at the B3LYP//B3LYP level of theory) was observed for the equatorial coordination mode. Furthermore, based on the results of previous studies,[27] only those η^2-ethylene adducts in which the ethylene C=C bond coordinates in the equatorial plane, as opposed to perpendicular to it, were examined. The resultant optimized structures of the two η^2-ethylene adduct isomers (**3a** and **3b**) are displayed in Figure 2.

At the CCSD(T)//B3LYP level of theory, a slight energetic preference, of 1.2 kcal/mol, was found for the mixed equatorial/axial (**ea**) bisphosphine η^2-ethylene adduct (isomer **3b**) over the bis-equatorial isomer (**ee**, isomer **3a**). On the other hand, the two isomers are predicted to be isoenergetic at the B3LYP//B3LYP levels of theory. The addition of ethylene to **2a** and **2b** is predicted to be exothermic by 21.5 (11.0) and 23.8 (12.1) kcal/mol, respectively. These predictions are in accord with the previous modeling studies, which found ethylene addition to the related HRh(PH₃)(CO)₂ catalyst to be exothermic by 24.8 and 32.2 kcal/mol, at the MP2//RHF level of theory.[31]

The saturated η^2-ethylene adducts adopt a trigonal bipyramidal geometry, and as expected, the coordination of ethylene induces a significant lengthening of the C=C bond from 1.369 Å in free ethylene to 1.434 Å for **3a** and 1.437 Å for **3b**. Furthermore, the coordination of ethylene to the active catalyst induces a slight shortening of the Rh–H bond by 0.03 Å and a slight lengthening of the Rh–P and Rh–CO bonds by 0.03–0.06 Å.

3. Olefin Insertion. In the next step of the hydroformylation catalytic cycle the olefin inserts into the Rh–H bond to generate an unsaturated Rh-alkyl complex. The B3LYP optimized geometries of the olefin insertion transition states (TSs) (**3a‡**, **3b₁‡**, and **3b₂‡**) originating from the two η^2-ethylene adducts are displayed in Figure 2, along with the corresponding Rh-ethyl products (**4a** and **4b**). In proceeding from the η^2-ethylene adducts to the olefin insertion TSs, the ethylene ligand must rotate out of the equatorial plane and shift upward in order for its methylene group to align with the axial hydride. As seen in Figure 2, the ethylene ligand in the TSs orients itself intermediary between a parallel and perpendicular alignment. Simultaneously, the axial hydride bends toward the incoming CH₂ group to expedite insertion. A total of three olefin insertion TSs were located at the B3LYP level: **3a‡** originating from the **ee** η^2-ethylene adduct, along with **3b₁‡** and **3b₂‡** originating from the **ea** η^2-ethylene adduct. The latter two transition states differ in the direction that the ethylene ligand rotates out of the equatorial plane. In **3b₁‡** the incoming CH₂ group is oriented toward the equatorial PH₃ ligand, while in **3b₂‡** it is oriented toward

(58) Frenz, B. A.; Ibers, J. A. In *The Hydride Series*; Muetterties, E. L., Ed.; Marcel Dekker: New York, 1971; Vol. 1.
(59) Rossi, A. R.; Hoffmann, R. *Inorg. Chem.* **1975**, *14*, 365.
(60) Kastrup, R. V.; Merola, J. S.; Oswald, A. A. *Adv. Chem. Ser.* **1982**, *196*, 43.
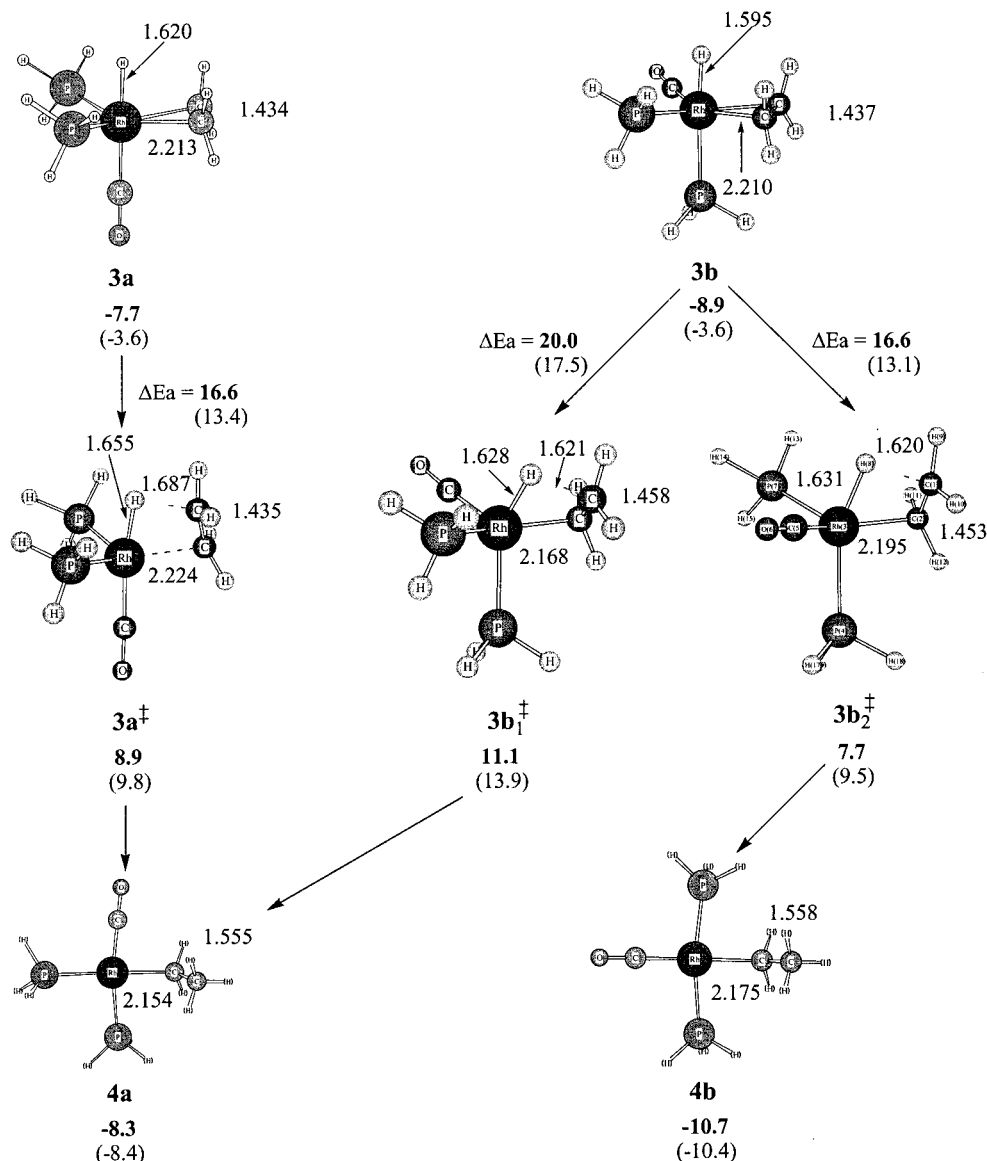
Figure 2. Predicted structural and energetic data for the species involved in the olefin addition and olefin insertion steps. Energy values given in bold correspond to the CCSD(T)//B3LYP relative energies (in kcal/mol), while those in parentheses correspond to the B3LYP//B3LYP relative energies. All geometric parameters were optimized at the B3LYP/SBK(d) level of theory. All distances are in angstroms, and angles in degrees.

the equatorial CO ligand. Harmonic vibrational frequency calculations confirmed that all three species are indeed transition states containing a single imaginary frequency (**3a**[‡] 712i cm^{−1}, **3b₁**[*] 912i cm^{−1}, and **3b₂**[‡] 824i cm^{−1}). In each case animation of the normal mode for the lone imaginary frequency displayed the desired nuclear displacements required for olefin insertion into the Rh−H bond. As evident from the structures of the TSs and confirmed by calculation of the IRC, **3a**[‡] and **3b₁**[‡] generate the cis Rh-ethyl insertion product (**4a**), while **3b₂**[‡] leads to the trans Rh-ethyl product (**4b**). This connectivity has also been corroborated recently by Rocha and de Almeida via an IRC calculation for the related propene insertion reaction.[61]

The olefin insertion reaction is predicted to be slightly exothermic by 0.6 (4.8) and 1.8 (6.8) kcal/mol, respectively, for the two pathways: **3a** → **4a** and **3b** → **4b**. The trans Rh-alkyl, **4b**, is predicted to be more stable,

by 2.4 (2.0) kcal/mol, than the cis isomer, **4a**. The activation barrier for the ethylene insertion pathway originating from the **ee** η^2-ethylene adduct, **3a** → **3a**[‡] → **4a**, was calculated to be 16.6 (13.4) kcal/mol, while the barriers for the alternate pathways originating from the **ea** η^2-ethylene adduct, **3b** → **3b₁**[‡] → **4a** and **3b** → **3b₂**[‡] → **4b**, were computed to be 20.0 (17.5) and 16.6 (13.1) kcal/mol, respectively. In **3b₁**[‡] there is a destabilizing interaction between the equatorial PH₃ ligand and the hydride ligand as it bends down toward the rotated ethylene, which is not present in **3b₂**[‡]. This unfavorable interaction results in an increased activation barrier for the olefin insertion reaction proceeding through **3b₁**[‡]. As the steric bulk of the phosphine ligands is increased, the repulsion between the hydride and the phosphine should increase further, thereby making the barrier to olefin insertion through **3b₁**[‡] even larger. Interestingly, the ethylene ligand in **3a**[‡] adopts an orientation that is closer to perpendicular in order to reduce the repulsion between the hydride ligand and the two equatorial

(61) Rocha, W. R.; de Almeida, W. B. *Int. J. Quantum Chem.* **2000**, *78*, 42.

phosphine ligands. Previous modeling studies[31] found the olefin insertion step in the related $HRh(PH_3)(CO)_2$-(η^2-C_2H_4) system to be more exothermic (12.0 kcal/mol at the MP2//RHF level of theory) and proceed with a larger activation barrier, of 21−23 kcal/mol, than found in the present study. However, in this study the transition state adopted a square pyramidal geometry, with the hydride and ethylene ligands occupying basal positions.

A comparison of the geometries of the species involved in the olefin insertion reaction indicates that the transition states occur early along the reaction coordinate. In the TS geometries (**3a**‡, **3b₁**‡, and **3b₂**‡) the Rh−H distance is increased by only 0.03−0.04 Å, while the Rh−C bond for the incoming CH_2 group, to which the hydride attaches, is stretched by only 0.1 Å with respect to their optimum values in the adduct complexes (**3a** and **3b**). In addition, there is only a small degree of rehybridization from sp^2 to sp^3 C−C bonding in the ethylene ligand as this distance is stretched by less than 0.02 Å upon going from the η^2-ethylene adduct (**3a** or **3b**) to the transition state (**3a**‡ or **3b₁,₂**‡). As expected, the saturated C−C bond in the Rh-alkyl products is more than 0.1 Å longer than the unsaturated C−C double bond of the η^2-ethlyene adducts. Furthermore, the Rh−C_{alkyl} bond is predicted to be 0.03−0.05 Å shorter than the Rh−$C_{ethylene}$ bond. These geometric changes are consistent with the conversion from an unsaturated alkene ligand to a saturated alkyl ligand.

4. CO Addition. Following the production of the unsaturated Rh-alkyl intermediates, the next step in the catalytic cycle involves the addition of CO to generate the saturated, 18-electron biscarbonyl trigonal bipyramidal compounds shown in Figure 3. Two CO addition product isomers differing in the arrangement of the PH_3 ligands were optimized. In **5a** the two PH_3 ligands have a mixed **ea** arrangement, while in **5b** both PH_3 ligands occupy equatorial sites (**ee**). Additionally, several conformers of these two isomers were located by rotating the alkyl ligand around the Rh−C bond. These conformers differed in the position of the alkyl methyl relative to the three equatorial ligands. For example by rotating around the Rh−C bond of **5b** another conformer with the alkyl methyl oriented between the equatorial CO ligand and one of the equatorial PH_3 ligands was obtained. All of these conformers were approximately isoenergetic to **5a** and **5b**; however, since the alignment of the equatorial CO to the α-C of the alkyl ligand is less optimal, it seems reasonable to propose that they are less likely to undergo the subsequent CO insertion step and they will not be discussed further. It should be added that optimizations were also initiated from complexes containing an equatorial ethyl ligand; however, in all cases these species rearranged to one of the stationary points containing an axially coordinated ethyl ligand.

The CO addition to **4a** and **4b** is predicted to be highly exothermic, by 21.8 (17.0) and 18.0 (13.8) kcal/mol, respectively. The **ea** isomer, **5a**, is predicted to be more stable, by 1.4 (1.2) kcal/mol, than the **ee** isomer, **5b**.

The addition of a CO ligand to the square-planar Rh-alkyl intermediates induces an increase in all of the Rh−L bonds. The increase is smaller (about 0.01−0.05 Å) for those ligands cis to the incoming CO ligand than that found for those ligands in the same equatorial plane as the incoming CO ligand (about 0.05−0.10 Å). The incoming CO ligand will compete with the other ligands in the equatorial plane for the same metal electron density, resulting in larger increases in the M−L bonds than found for those ligands that are cis to the incoming CO ligand.

5. CO Insertion. In the subsequent step of the catalytic cycle a CO ligand cis to the ethyl ligand inserts into the Rh−ethyl bond to generate a 16-electron, square-planar Rh-acyl species. The B3LYP optimized structures of the most stable Rh-acyl products (**6a** and **6b**) are displayed in Figure 3, along with the two TSs (**5a**‡ and **5b**‡) connecting them to the corresponding reactant complexes (**5a** and **5b**). The computed harmonic vibrational frequencies confirmed that **5a**‡ and **5b**‡ are indeed transition states on their respective potential energy hypersurfaces, each having a single imaginary frequency (**5a**‡ 268i cm⁻¹and **5b**‡ 258i cm⁻¹) whose normal mode exhibits the nuclear motions required for the CO insertion process.

At the CCSD(T)//B3LYP level, the CO insertion process is predicted to be endothermic by 9.1 and 9.2 kcal/mol for the two pathways **5a** + CO → **6a** and **5b** + CO → **6b**. On the other hand, the B3LYP//B3LYP calculations predict the CO insertion reaction following these two paths to be slightly exothermic, by 0.7 and 1.1 kcal/mol, respectively. The CCSD(T)//B3LYP results are in line with a number of earlier theoretical studies focusing on the CO insertion step in the $HCo(CO)_4$, CH_3-$Co(CO)_3$, and $HRh(CO)_4$ catalyst systems, which found this process to be endothermic by varying amounts, at a variety of different levels of theory.[15,19,25] Morokuma et al.[31] predicted two of the pathways for the CO insertion step in $Rh(PH_3)_2(CO)_2(CH_2CH_3)$ to be endothermic by 2.0 and 14.2 kcal/mol, at the MP2//RHF level. However, they located a third possible CO insertion pathway, which was predicted to be exothermic by 6.0 kcal/mol.

Energy barriers of 20.4 (14.9) and 22.7 (18.6) kcal/mol were predicted for the two possible CO insertion routes: **5a** → **5a**‡ → **6a** and **5b** → **5b**‡ → **6b**. The CCSD-(T)//B3LYP energy barriers are in good agreement with the previous MP2//RHF values of 21.5−26.1 kcal/mol of Morokuma et al.[31] Interestingly, the barriers predicted for CO insertion in the phosphine-modified Rh carbonyl catalyst systems are substantially higher than that predicted by Ziegler and co-workers[19] for the Co carbonyl catalyst system (9.6 kcal/mol at the local DFT level of theory).

In proceeding from the CO addition intermediates (**5a** and **5b**) to the CO insertion transition states (**5a**‡ and **5b**‡) the ethyl ligand bends down toward the equatorial CO ligand. This distortion is coupled with a bending of the oxygen atom of the CO ligand away from the incoming ethyl group in order to decrease the steric and electronic repulsion. In the TS structures the Rh−C_{ethyl} bond is about 0.35 Å longer than its value in **5a** and **5b**, while the C_{ethyl}−C_{CO} distance is quite short at 1.96 Å. This indicates that the CO insertion TSs tend to occur much later along the reaction coordinate than the olefin insertion TSs discussed earlier.

For the Rh-acyl products a slight preference was found for the syn conformation of the methyl group of
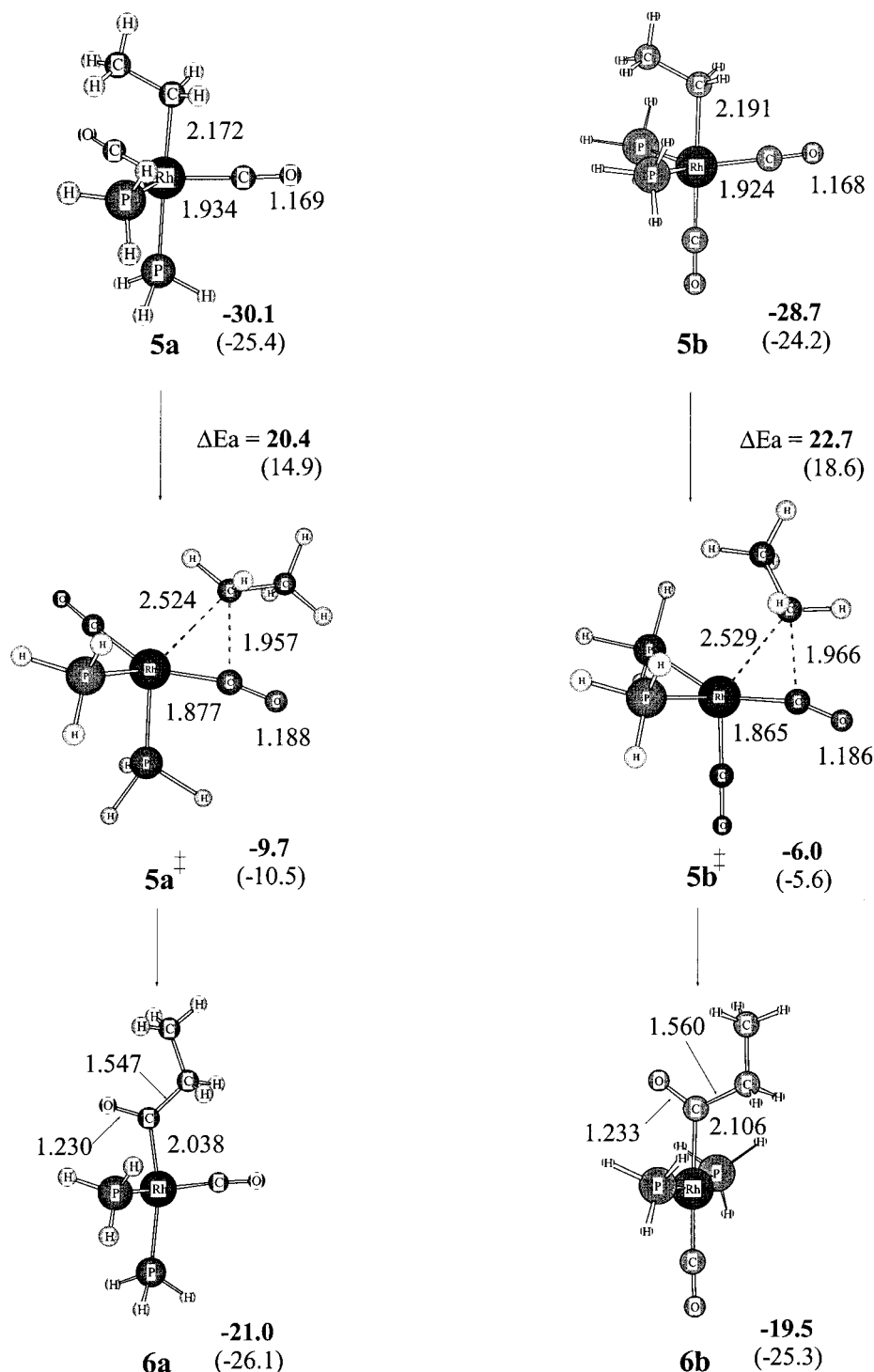
Figure 3. Predicted structural and energetic data for the species involved in the CO addition and CO insertion steps. Energy values given in bold correspond to the CCSD(T)//B3LYP relative energies (in kcal/mol), while those in parentheses correspond to the B3LYP//B3LYP relative energies. All geometric parameters were optimized at the B3LYP/SBK(d) level of theory. All distances are in angstroms, and angles in degrees.

the acyl ligand with respect to the acyl oxygen, in agreement with previous modeling studies.[31] Optimization of the anti conformers led to species that were either slightly higher in energy (by about 1 kcal/mol) than their syn counterparts or converged to the syn conformation. Interestingly, the $L_{eq}-Rh-L_{eq}$ bond angle in the **ea** Rh-acyl isomer (**6a**) deviates substantially from 180°, perhaps suggesting that there is some interaction between the acyl oxygen and the Rh center (the $Rh-O_{acyl}$ distance is 2.76 Å) that prevents the ligands from becoming perfectly trans to one another.

6. H₂ Oxidative Addition. Following generation of the unsaturated Rh-acyl intermediates, the next step in the catalytic cycle involves the oxidative addition of H_2 to generate a saturated six-coordinate Rh-acyl dihydride. Optimization of the H_2 oxidative addition products was initiated by adding H_2 to both faces of the Rh-acyl intermediates. The results from the present study show a clear preference for the oxidative addition of H_2 on the same side as the ethyl moiety of the acyl ligand over the addition on the same side as the acyl oxygen. The final H_2 oxidative addition product gener-
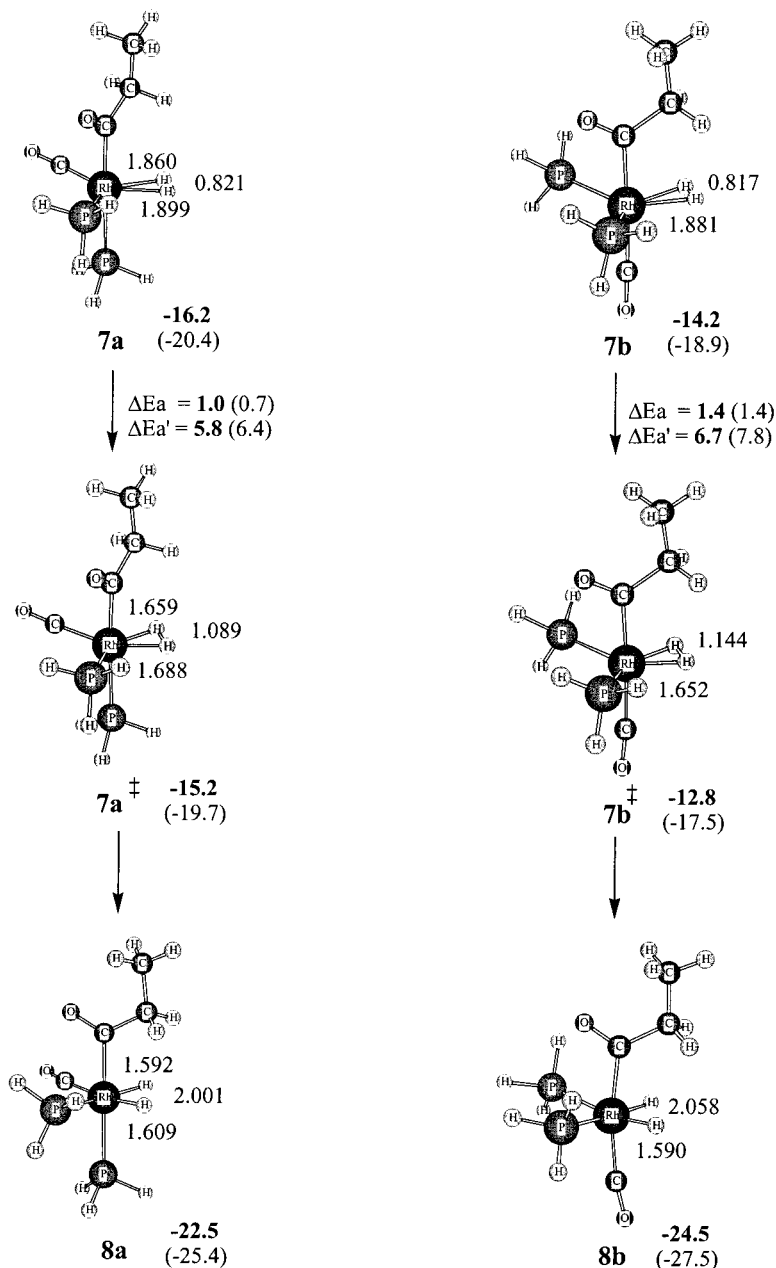
Figure 4. Predicted structural and energetic data for the species involved in the H₂ oxidative addition step. The set of energy barriers labeled as ΔE_a corresponds to the energy barrier predicted for the H₂ oxidative addition reaction proceeding from the η^2-H₂ adducts, while those labeled as $\Delta E_a'$ avoid the participation of these adducts in the reaction coordinate. Energy values given in bold correspond to the CCSD(T)//B3LYP relative energies (in kcal/mol), while those in parentheses correspond to the B3LYP//B3LYP relative energies. All geometric parameters were optimized at the B3LYP/SBK(d) level of theory. All distances are in angstroms, and angles in degrees.

ated via addition of H₂ on the same side as the acyl ethyl group of **6a** was found to be more stable, by 4.9 (4.4) kcal/mol, than the product formed via the addition on the opposite face. Furthermore, the activation barrier for the addition of H₂ on the same side as the ethyl group was predicted to be 3.3 (3.3) kcal/mol lower than the barrier for the addition on the same side as the acyl oxygen.

The B3LYP optimized molecular geometries of the most stable H₂ oxidative addition products, **8a** and **8b**, are given in Figure 4, along with the optimized geometries of the corresponding H₂ oxidative addition TSs, denoted as **7a‡** and **7b‡**. The structures of the two η^2-H₂ adducts located early along the H₂ oxidative addition reaction coordinate (denoted as **7a** and **7b**) are also

displayed in Figure 4. Hessian characterization of the η^2-H₂ adducts revealed that they are local minima on their respective potential energy surfaces, while each of the H₂ oxidative addition products contained a single negative eigenvalue. However, the magnitude of this negative Hessian eigenvalue was very small (with computed harmonic vibrational frequencies of 10−15i cm⁻¹), and the normal mode associated with it corresponded to a rotation of one or both of the PH₃ ligands. Since these PH₃ rotations are very floppy, no attempt was made to eliminate this mode since optimization along this mode should not lower the energies of these species significantly. The transition states **7a‡** and **7b‡** contained a single imaginary frequency (**7a‡** 911i cm⁻¹ and **7b‡** 998i cm⁻¹), the animation of which exhibited

the desired nuclear displacements for the H_2 oxidative addition process.

The H_2 oxidative addition product exhibiting a bis-equatorial arrangement of the two PH_3 ligands (**8b**) was found to be more stable, by 2.0 (2.1) kcal/mol, than the product containing an equatorial–axial arrangement of the two phosphines (**8a**). The reaction pathways for the oxidative addition of H_2, **6a** + H_2 → **8a** and **6b** + H_2 → **8b**, were predicted to be thermodynamically favorable by 1.5 (−0.7) and 5.0 (2.2) kcal/mol, respectively. The η^2-H_2 adducts (**7a** and **7b**) are predicted to lie 4.8 (5.7) and 5.3 (6.4) kcal/mol above the respective Rh-acyl intermediates, **6a** and **6b**, and free H_2. If the H_2 oxidative addition reaction is assumed to go through the η^2-H_2 adducts on their way to the transition states, only modest energy barriers of 1.0 (0.7) and 1.4 (1.4) kcal/mol are predicted for **6a** → **7a** → **7a**‡ → **8a** and **6b** → **7b** → **7b**‡ → **8b**. On the other hand, if the H_2 oxidative addition proceeds directly from the Rh-acyl intermediates to the transition states, avoiding the η^2-H_2 adducts, the activation barriers for these pathways are predicted to be 5.8 (6.4) and 6.7 (7.8) kcal/mol, respectively.

The current CCSD(T)//B3LYP energetics are in line with the previous MP2//RHF results of Morokuma and co-workers, who predicted the H_2 oxidative addition step to be slightly exothermic (by 4–7 kcal/mol) and to proceed with a barrier of 12–15 kcal/mol.[31] In their studies they did not locate the η^2-H_2 adducts, perhaps due to the neglect of electron correlation effects during the geometry optimizations. In their MP2 study of the rhodium carbonyl catalyst system Frenking et al.[25] located η^2-H_2 adducts along the H_2 oxidative addition reaction coordinate. However, they found these adducts to be slightly more stable than the initial Rh-acyl complexes (<1 kcal/mol) and predicted the H_2 oxidative addition to proceed with a very modest activation barrier of 2.7 kcal/mol. This indicates, as expected, that the dihydride complexes are less likely to form in the phosphine-substituted complexes than in the parent metal carbonyls.[20]

As the H_2 oxidative addition reaction progresses from the η^2-H_2 adducts to the TSs and finally to the H_2 oxidative addition products, there is a smooth progression as the H–H bond breaks and the Rh–H bond forms. The H–H bond length in the η^2-H_2 adducts is lengthened by only 0.05–0.08 Å from its B3LYP optimum value of 0.743 Å in free H_2. Continuing along the reaction coordinate from the η^2-H_2 adducts to the TSs there is a significant lengthening of the H–H bond, by about 0.3–0.4 Å, coupled with a significant shortening of the Rh–H bond, by about 0.2–0.4 Å. The H–H bond is further cleaved, while the Rh–H bond is shortened by about 0.05 Å in the final oxidative addition products. There appears to be a substantial degree of H–H bond breakage and Rh–H bond formation in the H_2 oxidative addition TSs, and they can therefore be classified as late TSs.

7. Aldehyde Reductive Elimination. The final step in Wilkinson's hydroformylation catalytic cycle is the irreversible reductive elimination of the aldehyde product. One of the hydride ligands in $EtC(O)Rh(PH_3)_2(CO)$-$(H)_2$ migrates to the acyl carbon, while simultaneously the Rh–C_{acyl} and the Rh–H bonds are cleaved to produce the desired aldehyde product and regenerate
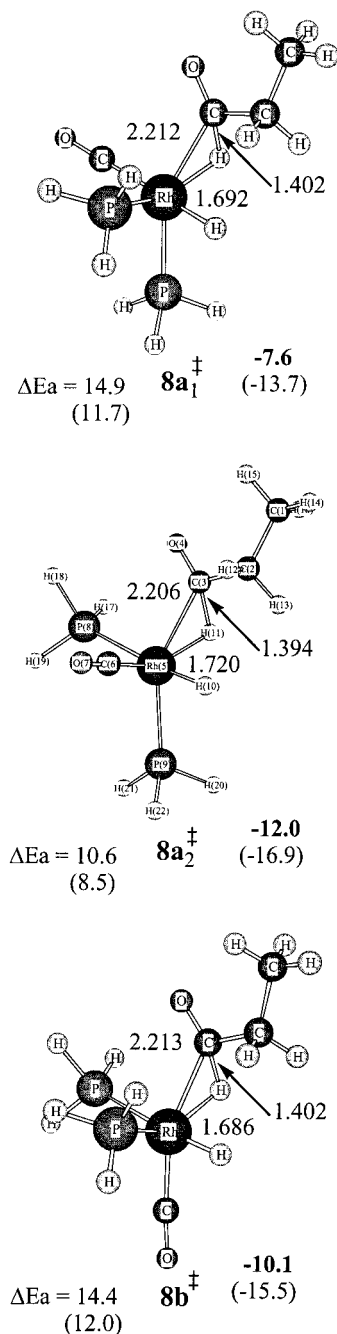

Figure 5. Structural and energetic data for the transition states of the aldehyde reductive elimination step. Energy values given in bold correspond to the CCSD(T)//B3LYP relative energies (in kcal/mol), while those in parentheses correspond to the B3LYP//B3LYP relative energies. All geometric parameters were optimized at the B3LYP/SBK-(d) level of theory. All distances are in angstroms, and angles in degrees.

the active catalyst species. Proceeding from the most stable H_2 oxidative addition products, **8a** and **8b**, a total of three aldehyde reductive elimination transition states were located, two originating from **8a** (denoted as **8a$_1$**‡ and **8a$_2$**‡) and one originating from **8b** (denoted as **8b**‡). Their optimized geometries are displayed in Figure 5. The two transition states originating from **8a** are generated by allowing each of the inequivalent hydride ligands to migrate to the acyl carbon. In **8a$_1$**‡, the hydride ligand trans to the PH_3 ligand migrates, while in **8a$_2$**‡ the hydride ligand trans to the CO ligand

migrates. Harmonic vibrational frequency characterization of these three stationary points confirmed that they are indeed transition states with a single imaginary eigenvalue ($8a_1^{\ddagger}$ 569i cm^{-1}, $8a_2^{\ddagger}$ 437i cm^{-1}, $8b^{\ddagger}$ 557i cm^{-1}), whose normal mode displayed the desired nuclear displacements for aldehyde reductive elimination.

The structures of $8a_1^{\ddagger}$ and $8a_2^{\ddagger}$ indicate that the aldehyde reductive elimination reaction proceeding from the mixed **ea** H$_2$ oxidative addition product **8a** is capable of regenerating the trans (**2a**) and cis (**2b**) isomers of the active catalyst, respectively. Therefore, in addition to the two pathways that regenerate the same isomer of the active catalyst upon aldehyde reductive elimination (i.e., $8a \rightarrow 8a_1^{\ddagger} \rightarrow 2a + HC(O)CH_2CH_3$ and $8b \rightarrow 8b^{\ddagger} \rightarrow 2b + HC(O)CH_2CH_3$) there is another pathway which starts with the trans catalyst (**2a**) and then generates the cis catalyst (**2b**) at the end of the catalytic cycle (i.e., $8a \rightarrow 8a_2^{\ddagger} \rightarrow 2b + HC(O)CH_2CH_3$). At the CCSD(T)//B3LYP level of theory these three aldehyde reductive elimination pathways are predicted to be endothermic by 11.9, 15.0, and 13.0 kcal/mol, respectively. Meanwhile, all of the paths are predicted to be thermally neutral when computed from the B3LYP//B3LYP energies.

The energy barriers for the two paths that regenerate the same initial catalyst isomer species are predicted to be 14.9 (11.7) and 14.4 (12.0) kcal/mol. The predicted activation barrier for the pathway through $8a_2^{\ddagger}$, which generates the cis catalyst from the initial trans isomer, is predicted to be 10.6 (8.5) kcal/mol. The energy barrier for the migration of a hydride ligand which is trans to a CO ligand ($8a_2^{\ddagger}$) is predicted to be 3–4 kcal/mol lower than that for the migration of a hydride ligand trans to a PH$_3$ ligand ($8a_1^{\ddagger}$ and $8b^{\ddagger}$), in accord with the larger trans influence of the CO ligand with respect to that of a phosphine ligand.

The CCSD(T)//B3LYP energetic predictions of the present study are in quite good agreement with the previous MP2//RHF modeling studies by Morokuma et al., who found the aldehyde reductive elimination to be endothermic by 7.1 kcal/mol and found a barrier of 11.3 kcal/mol for this process.[31] Interestingly, they found the aldehyde reductive elimination proceeds through an η^2-aldehyde adduct that lies 1.7 kcal/mol below the corresponding Rh-acyl dihydride intermediate. Further modeling studies by Ziegler et al.[24] and Frenking and co-workers[25] on the HCo(CO)$_4$ and HRh(CO)$_4$ catalyst systems also found the final aldehyde reductive elimination step to be an endothermic process, by about the same magnitude as the CCSD(T)//B3LYP values.

In the aldehyde reductive elimination TSs the hydride ligand that migrates to the acyl carbon bends significantly out of the equatorial plane toward the axial acyl group, while simultaneously the acyl ligand, as a whole, bends downward toward the equatorial plane to facilitate the migration, as indicated in Figure 5. Although the geometries of the TSs suggest that there is a significant amount of C–H bond formation, with a C–H bond length of only 1.40 Å (compared to its optimum value of 1.09 Å in the aldehyde product) and a small H–Rh–C bond angle of 39°, the Rh–C$_{acyl}$ and Rh–H bonds are only 0.1 Å longer in the TS structures than in the respective Rh-acyl dihydride intermediates. Hence, it is difficult to assess how far along the aldehyde

reductive elimination reaction coordinate the transition states are positioned.

8. Complete Catalytic Cycle. The complete gas-phase potential energy hypersurface for the hydroformylation of ethylene using a HRh(PH$_3$)$_2$(CO) active catalyst may be constructed by combining the results from each of the individual steps described above. In the following discussion only the CCSD(T)//B3LYP values will be discussed.

Beginning with the initial PH$_3$ dissociation step, we predicted a slight energetic preference for the trans isomer of the active catalyst (**2a**) over the cis isomer (**2b**) of 1.1 kcal/mol, at both the CCSD(T)//B3LYP and B3LYP//B3LYP levels of theory. As the steric bulk of the PR$_3$ ligands is increased from the model PH$_3$ ligand to one of the larger experimental ligands commonly employed, the trans–cis energy difference should increase further. If one assumes that both PH$_3$ dissociation pathways are plausible, the olefin adduct (**3b**) produced from the less stable cis catalyst species is predicted to be more stable, by 1.2 kcal/mol, than the olefin adduct (**3a**) produced from the trans catalyst species. However, the barrier for the subsequent olefin insertion step originating from the more stable olefin adduct (**3b**) through transition state $3b_1^{\ddagger}$ is predicted to be 3.4 kcal/mol larger than that which proceeds through $3b_2^{\ddagger}$. It is also 3.4 kcal/mol higher than the alternative olefin insertion pathway originating from the less stable olefin adduct, **3a**, and going through $3a^{\ddagger}$. Hence, the pathway that must traverse the larger energetic barrier for olefin insertion through transition state $3b_1^{\ddagger}$ can be neglected. As a result of this large barrier, in proceeding from **3b** the olefin will be forced to rotate out of the equatorial plane in only one direction, toward the smaller CO ligand, and will therefore proceed through $3b_2^{\ddagger}$ only. Alternatively, the trigonal bipyramidal olefin adduct **3b** can undergo a Berry pseudorotation to convert to **3a**, thereby enabling the olefin insertion to proceed through $3a^{\ddagger}$. In their previous study Morokuma et al. predicted a barrier of around 10 kcal/mol for such a rearrangement in the related HRh(PH$_3$)(CO)(C$_2$H$_4$) system.[27]

The resultant trans Rh-ethyl intermediate (**4b**) which evolved from $3b_2^{\ddagger}$ is predicted to be more stable than the cis Rh-ethyl intermediate (**4a**) produced from $3a^{\ddagger}$; however, the exothermicity of the two routes are predicted to be roughly the same, 1.8 and 0.6 kcal/mol for $3b \rightarrow 3b_2^{\ddagger} \rightarrow 4b$ and $3a \rightarrow 3a^{\ddagger} \rightarrow 4a$, respectively. The subsequent CO additions to **4a** and **4b** to yield **5a** and **5b** are predicted to be strongly exothermic, by 21.8 and 18.0 kcal/mol, respectively. However, the subsequent barrier for CO insertion into the Rh–ethyl bond of **5b**, via $5b^{\ddagger}$, is predicted to be 2.3 kcal/mol higher than the barrier for CO insertion into the Rh–ethyl bond of **5a**, proceeding through $5a^{\ddagger}$. Hence, in all likelihood intermediate **5b** will undergo a molecular rearrangement, via Berry pseudorotation, to convert to **5a**, since the barrier for this rearrangement will be less than the 22.7 kcal/mol required for CO insertion. The catalytic cycle would then proceed from the mixed **ea** isomer, **5a**, to the cis Rh-acyl intermediate, **6a**, by passing through $5a^{\ddagger}$, which has a smaller energy barrier of 20.4 kcal/mol. At this stage all of the possible reaction paths originating from the cis catalyst, **2b**, have been elimi-
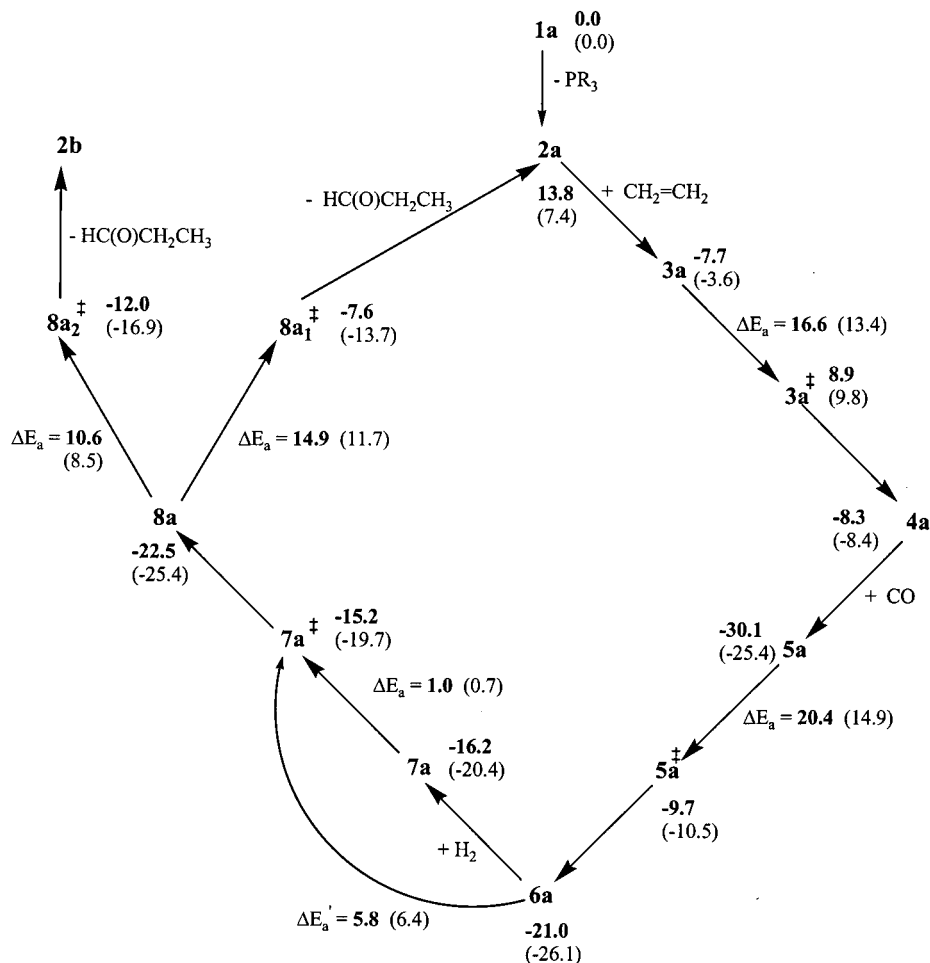
Figure 6. The preferred pathway for ethylene hydroformylation catalyzed by HRh(PH$_3$)$_2$(CO). Relative energy values given in bold correspond to those predicted at the CCSD(T)//B3LYP level of theory, while the values given in parentheses correspond to those predicted at the B3LYP/SBK(d) level of theory.

nated, leaving only those originating from the trans catalyst, **2a**, to be considered from this point on.

A preference was found for the oxidative addition of H$_2$ to **6a** on the same side as the acyl ethyl moiety over the addition on the same side as the acyl oxygen. Proceeding from the most stable H$_2$ oxidative addition intermediate, **8a**, there are two possible pathways for aldehyde reductive elimination, **8a** → **8a$_1$‡** → **2a** + HC-(O)CH$_2$CH$_3$ and **8a** → **8a$_2$‡** → **2b** + HC(O)CH$_2$CH$_3$, depending on which hydride ligand migrates to the acyl carbon. At both levels of theory employed, an energetic preference was found for the hydride ligand trans to the CO ligand to migrate to the acyl carbon, as opposed to the hydride that is trans to the PH$_3$ ligand, in agreement with that expected based on the stronger trans influence of the CO ligand. Such a migration leaves the remaining hyride ligand trans to the PH$_3$ ligand and therefore generates the cis isomer (**2b**) of the active catalyst. Therefore, an additional step is needed to convert from the less favorable catalytic cycle originating from the cis catalyst species (**2b**) to the favored catalytic cycle initiated from the trans catalyst (**2a**). This interconversion would in all likelihood occur via a Berry pseudorotation of a trigonal bipyramidal intermediate species, either the η^2-ethylene adduct (**3b**) or the CO addition intermediate (**5b**). Morokuma has previously shown that such an interconversion is quite facile, and they predicted a modest barrier of about 10 kcal/mol for

the Berry pseudorotation interconversion of the HRh-(PH$_3$)(CO)$_2$(C$_2$H$_4$) η^2-olefin adducts. If the alternative aldehyde reductive elimination pathway, in which the hydride trans to the phosphine, undergoes the migration, it is predicted to proceed with a larger barrier, by about 4 kcal/mol. However, since it regenerates the trans isomer of the active catalyst, no further interconversion step needs to be invoked for the second go-round of the catalytic cycle. The energetic ordering of the two elimination TSs may be altered by the influence of more realistic phosphine ligands or environmental effects such as solvent. Alternatively, these results, when viewed in light of previous research, may be indicative of the importance of pseudorotation processes in the hydroformylation catalytic cycle.

According to the current CCSD(T)//B3LYP calculations, one can envision two preferred pathways for ethylene hydroformylation catalyzed by the model HRh-(PH$_3$)$_2$(CO) system, differing only in the final aldehyde reductive elimination step, as shown in eqs 2 and 3 and displayed schematically in Figure 6.

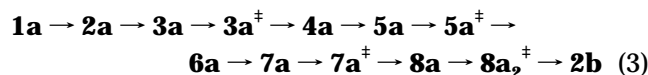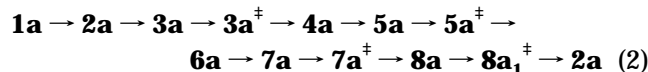$$1a \rightarrow 2a \rightarrow 3a \rightarrow 3a^‡ \rightarrow 4a \rightarrow 5a \rightarrow 5a^‡ \rightarrow$$
$$6a \rightarrow 7a \rightarrow 7a^‡ \rightarrow 8a \rightarrow 8a_1^‡ \rightarrow 2a \quad (2)$$

$$1a \rightarrow 2a \rightarrow 3a \rightarrow 3a^‡ \rightarrow 4a \rightarrow 5a \rightarrow 5a^‡ \rightarrow$$
$$6a \rightarrow 7a \rightarrow 7a^‡ \rightarrow 8a \rightarrow 8a_2^‡ \rightarrow 2b \quad (3)$$

Table 1. Dependence of the Calculated Activation Barriers (ΔE_a, in kcal/mol) on the H Atom Basis Set Employed

method[a]	ΔE_a (Ol. Ins.)	ΔE_a (CO Ins.)	ΔE_a (H₂ Add.)	ΔE_a (Ald. RE)
B3LYP/SBK(d)	13.4	14.9	6.4	11.7
B3LYP/SBK(d,p)	12.5	14.6	3.8	10.8

[a] The energies of the species were computed at the B3LYP level of theory employing one of the two SBK basis sets. The species were fixed at their B3LYP/SBK(d) optimized molecular geometries (i.e., B3LYP/SBK(d,p)//B3LYP/SBK(d) and B3LYP/SBK(d)//B3LYP/SBK(d) approaches).

These two preferred pathways contain no overly large activation barriers to impede the progress of the catalytic cycle nor do they have any deep thermodynamic wells to trap the catalytic cycle.

As seen in Figure 6, the rate-determining step is predicted to be the CO insertion step in the preferred hydroformylation catalytic cycle, at both levels of theory employed. Interestingly, most experimental studies[8,9] suggest that the rate-determining step for Rh-catalyzed hydroformylation is H₂ oxidative addition, while previous computational work on Rh-phosphine systems suggests that CO insertion is rate-determining. In the present study, the barrier for the H₂ oxidative addition step is predicted to be smaller than the barrier for the CO insertion step by a factor of 3 at the CCSD(T)// B3LYP level (by a factor of 2 at the B3LYP//B3LYP level of theory). These results are in line with the previous studies by Morokuma et al.[31] on the related HRh(PH₃)-(CO)₂ catalyst system. Perhaps this difference may be attributed to a deficiency in our computational methodology, particularly since the basis set employed for the hydrogen atoms was of double-ζ quality and contained no p polarization functions. To address this issue, the activation barriers for the olefin insertion, CO insertion, H₂ oxidative addition, and aldehyde reductive elimination elementary reactions of the preferred pathway were recomputed at the B3LYP level using an expanded triple-ζ plus polarization (TZVp) quality hydrogen basis set (namely 6-311G**[62]), which will be denoted here after as SBK(d,p). The results of these calculations are displayed in Table 1. Note that the geometric structures of the various intermediates and transition states were fixed at their original B3LYP/SBK(d) geometries (i.e., the B3LYP/SBK(d,p)//B3LYP/SBK(d) method) and the energies were corrected using the zero-point energies computed at the B3LYP/SBK-(d) level. As seen in Table 1, expanding the H atom basis set to TZVp quality induces only minor reductions, of 0.3−2.6 kcal/mol, in the B3LYP/SBK(d) computed activation barriers. The energy barrier for CO insertion, not surprisingly, changes the least (0.3 kcal/mol) upon augmenting the H atom basis set, since hydrogens play only a minor role in the TS. The barrier for H₂ oxidative addition is reduced the most (2.6 kcal/mol) since the two H atoms of the H₂ molecule are intimately involved in the reaction coordinate. The energy barriers for the olefin insertion and aldehyde reductive elimination are decreased by 0.9 and 1.0 kcal/mol, respectively, intermediate between the two extremes and in line with the fact that a single H atom is undergoing migration in

(62) Krishnan, R.; Binkley, J. S.; seeger, R.; Pople, J. A. *J. Chem. Phys.* **1980**, *72*, 650.

the transition states of both of these reactions. In general, the overall picture for the energetics of the catalytic cycle is not altered by increasing the size of the H atom basis set, thereby giving support to our original CCSD(T)/SBK(d)//B3LYP/SBK(d) and B3LYP/SBK(d)//B3LYP/SBK(d) computed energies. Alternatively, this difference between theory and experiment may be attributed to the neglect of solvent effects in the calculations, which might contribute to the activation barrier. Of the four elementary reactions investigated in detail in the current study, only the H₂ oxidative addition involves an unsaturated reactant complex. Assuming that each of the transition states for the four elementary reaction are stabilized to the same degree by the solvent, the solvent stabilization of this unsaturated complex will increase the activation barrier for the H₂ oxidative addition to a larger degree than for the remaining three elementary reactions. In fact, Morokuma et al.,[31] employing a single ethylene molecule as a model of the ethylene solvent, computed a large increase in the activation barrier for H₂ oxidative addition such that it was actually close to the same magnitude as the rate-limiting CO insertion reaction barrier. Our group is currently investigating this issue further, in which we are employing a more elaborate computational scheme in order to account for the effects of the solvent, both from a microsolvation and a bulk solvation viewpoint.

As mentioned at the outset of this paper, one of the goals of the current work was to enable a comparison between the ethylene hydroformylation process catalyzed by the two closely related HRh(PH₃)₂(CO) and HRh(PH₃)(CO)₂ catalyst systems. Although, a direct comparison of the two ethylene hydroformylation potential energy hypersurfaces computed by us for HRh-(PH₃)₂(CO) and by Morokuma et al.[31] for HRh(PH₃)-(CO)₂ is not entirely valid given the different computational methods employed, it is interesting to compare the two qualitatively. It should be mentioned that the two catalytic cycles differ chemically for only the first four elementary steps: catalyst generation, olefin addition, olefin insertion, and CO/PH₃ addition. The same chemical intermediates are involved for the final three steps of the catalytic cycle (CO insertion, H₂ oxidative addition, and aldehyde reductive elimination); hence the differences in these final steps reflect only differences in the computational approach employed. As expected, the potential energy hypersurfaces for these final three steps are qualitatively very similar. Focusing on the chemically different elementary reactions reveals that the computed activation barrier and thermodynamic values are very similar, qualitatively, for the first four elementary reactions. For both HRh(PH₃)$_m$(CO)$_n$ catalyst systems, the CO insertion step is predicted to be rate-limiting, while the activation barrier for the H₂ oxidative addition reaction is predicted to be very modest. One of the largest discrepancies between the two potential energy hypersurfaces is the size of the difference between the olefin insertion and CO insertion activation barriers. In the HRh(PH₃)₂(CO) catalyst system the energy barrier for olefin insertion is only 2 kcal/mol lower than the barrier of the rate-limiting CO insertion, while in the HRh(PH₃)(CO)₂ system the difference between the two insertion barriers is much

larger at 6 kcal/mol. The larger relative size of the olefin insertion barrier in the bisphosphine system may be attributed to the higher degree of steric crowding in the olefin insertion transition state than that found in the olefin insertion transition state for the monophosphine system.

The potential energy hypersurface of the ethylene hydroformylation process catalyzed by $HCo(CO)_4$ was constructed by Ziegler et al.[19–24] and it differs substantially from that of the current $HRh(PH_3)_2(CO)$ catalyst system. In the cobalt system, the initial catalyst generation step is predicted to be the rate-determining step, and it was predicted to be much more endothermic than the PH_3 dissociation step in the rhodium catalyst studied here. However, once the active catalyst species is generated, the CO insertion barrier was predicted to have the next highest energy barrier. The most significant difference between the cobalt and rhodium catalyst cycles is in the energy barrier for the olefin insertion step. In the cobalt system the activation barrier for the olefin insertion step is predicted to be very modest (1 kcal/mol), while in the rhodium system this barrier is predicted to be much higher (16.6 kcal/mol). This difference reflects the degree of steric crowding in the olefin insertion transition state and is in line with the observed higher degree of selectivity of the phosphine-modified rhodium catalyst system.
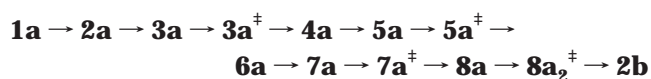
The energy difference between the aldehyde product, $HC(O)CH_2CH_3$, and the initial components of the hydroformylation reaction, C_2H_4, CO, and H_2, is referred to as the energy of hydroformylation (ΔE^{Hyf}). From the B3LYP energies a value of -34.7 kcal/mol was calculated for ΔE^{Hyf}, much more exothermic than the experimental ΔH^{Hyf} value of -28 kcal/mol.[63] However, a ΔE^{Hyf} value of -24.4 kcal/mol, in much better agreement with experiment, was obtained by recomputing the energies at the CCSD(T) level of theory.

Finally, since the complete ethylene hydroformylation catalytic cycle potential energy hypersurface has been calculated at the CCSD(T)//B3LYP and B3LYP//B3LYP levels of theory, it is possible to ascertain what changes are induced from a refinement of the energies at the higher CCSD(T) level. As seen in Figure 6, refinement of the energy of each species at the CCSD(T) level induces only minor changes in the activation barriers for each step of the catalytic cycle. In general, the CCSD(T)//B3LYP energy barriers are 2.7–4.5 kcal/mol larger than the corresponding B3LYP//B3LYP values. The barrier for the H_2 oxidative addition step is an exception, since the B3LYP//B3LYP value is decreased by 0.6 kcal/mol when the energies are recomputed at the CCSD(T)//B3LYP level. On the other hand, the thermodynamics of a number of the elementary steps of the catalytic cycle change significantly when recomputed based on the CCSD(T) energies. For the PH_3 dissociation, olefin addition, and CO addition steps the CCSD(T) calculations magnify the degree of endothermicity or exothermicity predicted at the B3LYP//B3LYP level. For the two migratory insertion steps (olefin insertion and CO insertion) and the aldehyde reductive elimination step the changes are more dramatic. The B3LYP//B3LYP calculations predict the olefin insertion step to be
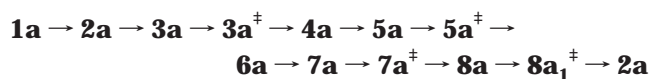
slightly exothermic, by 4.8 kcal/mol, while this step is predicted to be isoenergetic based on the CCSD(T) energies. The CO insertion step is predicted to be endothermic, by 9.1 kcal/mol, at the CCSD(T)//B3LYP level, while at the B3LYP//B3LYP level this step is predicted to be thermally neutral. The aldehyde reductive elimination step is predicted to be exothermic by 6.3 kcal/mol at the B3LYP//B3LYP level, while this step is predicted to be endothermic, by 7.0 kcal/mol, when the energies are computed at the CCSD(T) level. Although the thermodynamics of the elementary reactions are altered, the trends among the various possible pathways remain the same, independent of which method was employed to compute the energies of the various species involved in the catalytic cycle.

Summary and Conclusions

The potential energy hypersurface for ethylene hydroformylation catalyzed by $HRh(PH_3)_2(CO)$ was thoroughly mapped out at the CCSD(T)//B3LYP and B3LYP//B3LYP levels of theory. The preferred pathway for the catalytic cycle was found to originate from the trans isomer (**2a**) of the active catalyst. The alternative pathways originating from the cis isomer of the active catalyst (**2b**) were found to be less favorable due to significantly higher barriers for the olefin insertion and CO insertion steps. These large barriers stem primarily from unfavorable steric interactions between the migrating axial ligand and the spectator equatorial phosphine ligands. Of the possible reaction pathways initiated from the trans catalyst species (**2a**), a preference was found for the oxidative addition of H_2 on the same side as the ethyl moiety of the acyl ligand in the unsaturated Rh-acyl complex. In the subsequent aldehyde reductive elimination reaction, an energetic preference was found for the migration of the hydride ligand trans to the equatorial CO, even though this leads to the generation of the cis catalyst (**2b**) instead of the original trans isomer (**2a**).

$$\mathbf{1a} \rightarrow \mathbf{2a} \rightarrow \mathbf{3a} \rightarrow \mathbf{3a}^{\ddagger} \rightarrow \mathbf{4a} \rightarrow \mathbf{5a} \rightarrow \mathbf{5a}^{\ddagger} \rightarrow$$
$$\mathbf{6a} \rightarrow \mathbf{7a} \rightarrow \mathbf{7a}^{\ddagger} \rightarrow \mathbf{8a} \rightarrow \mathbf{8a_2}^{\ddagger} \rightarrow \mathbf{2b}$$

This implies that there must be some interconversion between the catalytic cycles originating from the two different active catalyst isomers, **2a** and **2b**, probably via a Berry pseudorotation for the trigonal bipyramidal η^2-olefin adducts (**3b**) or the CO addition intermediates (**5b**). Alternatively, if only those pathways that regenerate the same isomer of the active catalyst species are considered, the barrier for the final aldehyde reductive elimination step is predicted to be 3–4 kcal/mol higher; however, no interconversion between the catalytic cycles for different isomers is required, and the preferred pathway can be written as

$$\mathbf{1a} \rightarrow \mathbf{2a} \rightarrow \mathbf{3a} \rightarrow \mathbf{3a}^{\ddagger} \rightarrow \mathbf{4a} \rightarrow \mathbf{5a} \rightarrow \mathbf{5a}^{\ddagger} \rightarrow$$
$$\mathbf{6a} \rightarrow \mathbf{7a} \rightarrow \mathbf{7a}^{\ddagger} \rightarrow \mathbf{8a} \rightarrow \mathbf{8a_1}^{\ddagger} \rightarrow \mathbf{2a}$$

Both of these preferred pathways exhibit no overly large barriers or thermodynamic wells that would hinder the catalytic cycle.

At both the CCSD(T)//B3LYP and B3LYP//B3LYP levels, the CO insertion step is predicted to be the rate-

(63) Cornils, B. In *New Syntheses with Carbon Monoxide*; Falbe, J., Ed.; Springer-Verlag: New York, 1980.

determining step of the ethylene hydroformylation catalytic cycle, with a calculated activation barrier of 20.4 (14.9) kcal/mol. Although, these results are in line with those from previous theoretical studies, they do not agree with the available experimental evidence, which suggests that the H_2 oxidative addition step is rate limiting.[8,9] This deviation is believed to be due to the neglect of solvation effects in the calculations, which should increase ΔE_a for the H_2 oxidative addition relative to the other elementary steps. This step is the only one in the catalytic cycle that contains an unsaturated reactant complex that may be solvated to a significant degree, thereby increasing the activation barrier, as has been found by Morokuma et al.[31] in earlier work on related systems. Work is currently under way in our lab to further investigate the role solvation has on the hydroformylation process, employing a number of elaborate computational schemes to model the solvent.

A comparison of the calculated potential energy hypersurfaces for ethylene hydroformylation catalyzed by $HRh(PH_3)_2(CO)$, at the CCSD(T)//B3LYP level, and $HRh(PH_3)(CO)_2$, at the MP2//RHF level,[31] reveals that they are qualitatively very similar. The CO insertion step is predicted to be the rate-determining step in both catalytic cycles, while the H_2 oxidative addition step is predicted to occur with a very modest barrier. The most significant difference between the two catalytic cycle potential energy hypersurfaces is the size of the difference between the olefin insertion and CO insertion energy barriers. The larger steric crowding in the olefin insertion transition state for the bisphosphine catalyst system contributes to a larger activation barrier for the olefin insertion reaction relative to that for the rate-limiting CO insertion reaction. Further comparison of these potential energy hypersurfaces for the $HRh(PH_3)_m(CO)_n$ catalyst systems to that predicted for the $HCo(CO)_4$ catalyst system at the DFT level[19–24] shows, not surprisingly, a number of significant differences. The initial catalyst generation step, via CO dissociation, was found to be the rate-determining step in the cobalt carbonyl catalytic cycle. However, once the active catalyst is generated, the CO insertion step has the largest activation barrier, in agreement with the findings for the phosphine-modified rhodium carbonyl catalyst systems. Another interesting difference between the cobalt and rhodium catalytic cycles is the olefin insertion barrier, which was predicted to be very small (1 kcal/mol) for the cobalt system and much larger (17 kcal/mol) for the rhodium-phosphine system, reflecting the much larger steric demands of the phosphine ligands with respect to the carbonyl ligands.

At the B3LYP//B3LYP level of theory the energy of hydroformylation, ΔE^{HyF} (i.e., the energy difference between the end aldehyde product and the reactant

components: C_2H_4, CO, and H_2), is predicted to be −34.7 kcal/mol, which overestimates the experimental enthalpy of hydroformylation, ΔH^{HyF}, value of −28 kcal/mol.[62] However, a refinement of the energies at the CCSD(T) level yields a ΔE^{HyF} value of −24.4 kcal/mol, in much better agreement with the experimental ΔH^{HyF} value.

In addition to altering the ΔE^{HyF} value, recalculation of the energies of the intermediates and transition states participating in the ethylene hydroformylation process at the CCSD(T) level of theory has a profound effect on the energetics of the catalytic cycle. For the most part, the energetic barriers for the elementary reactions are only slightly modified from their B3LYP//B3LYP values. The barriers predicted at the CCSD(T)//B3LYP level are typically 2−4 kcal/mol higher than those predicted at the B3LYP//B3LYP level. On the other hand, CCSD(T) refinement of the energies has a much larger effect on the thermodynamics predicted for a number of the elementary steps in the catalytic cycle, particularly, the two migratory insertions and the aldehyde reductive elimination steps. The olefin insertion step, which was predicted to be slightly exothermic based on the B3LYP//B3LYP energies, was predicted to be thermally neutral at the CCSD(T) level. The CO insertion and aldehyde reductive elimination steps, which were predicted to be slightly exothermic or thermally neutral at the B3LYP//B3LYP level, were predicted to be endothermic by 9 and 7 kcal/mol, respectively, at the CCSD(T)//B3LYP level of theory. For the remaining steps, the CCSD(T)//B3LYP method tends to amplify the endothermicity or exothermicity of the elementary reactions with respect to their B3LYP//B3LYP values.